REFLECT DELIVERABLE D4.4

Numerical modelling of the geochemical behaviour of hot (type-A) and saline (type-C) fluids and validation against new data

Summary:

This document presents the application of coupled hydrogeochemical codes to the modelling of geothermal fluid reactivity in tubings during the production of geothermal energy. Two codes are used on two examples of fluids: one is very concentrated with a moderate temperature (no phase changes during the pumping) and one hot fluid with a lower salinity (with phase change). Results focus on the risks of scaling during the exploitation.

Authors:

Laurent André, BRGM, French Geological Survey
Cyprien Soulaine, ISTO
Pejman Shoeibi Omrani, TNO, Senior scientist

This project has received funding from the European Union's Horizon 2020 research and innovation programme under grant agreement nº 850626.

Title:	Numerical modelling of the geochemical behaviour of hot (type-A) and saline (type-C) fluids and validation against new data
Lead beneficiary:	BRGM
Other beneficiaries:	TNO
Due date:	April 2023
Nature:	Public
Diffusion:	All project partners and general public
Status:	Final
Document code:	REFLECT_D4.4
DOI:	https://doi.org/10.48440/gfz.4.8.2023.006
License information:	CC-BY 4.0
Recommended citation:	André L., Soulaine C., Omrani, P.S. (2023). The H2020 REFLECT project: Deliverable 4.4 - Numerical modelling of the geochemical behaviour of hot (type-A) and saline (type-C) fluids and validation against new data, *GFZ German Research Centre for Geoscience,* DOI: *https://doi.org/10.48440/gfz.4.8.2023.006*

Revision history	Author	Delivery date	Summary of changes and comments
Version 01	André et al.	21/04/2023	First draft
Version 02	André et al.	26/04/2023	Inclusion of galena in model upon comments from reviewers. Indication of sites from which the studies were inspired

Approval status			
	Name	Function	Date
Deliverable responsible	Laurent ANDRE	Hydrogeochemist (BRGM)	21/04/2023
WP leader	Laurent ANDRE	Hydrogeochemist (BRGM)	21/04/2023
Project Coordinator	Katrin Kieling	Project manager (GFZ)	26.04.2023

TABLE OF CONTENTS

FIGURES

TABLES

1 EXECUTIVE SUMMARY

One of the most important issue impacting almost all deep geothermal operations in the world is the in-situ chemical reactivity of the geothermal fluids leading most often to mineral precipitation and clogging risks. In order to maximise the technical feasibility, operational efficiency and economic returns of geothermal power plants, it is then vital that these systems work well for long periods without requiring significant maintenance.

To avoid treating these deleterious physical and chemical reactions and their consequence on production operations, we need to use relevant numerical tools in order to predict these processes and to anticipate them before they occur.

An accurate prediction of the scaling amount and location in the geothermal systems depends heavily on (1) characterization of the geothermal fluid, which is impacted by the uncertainties in the fluid sampling and analysis and (2) interaction between flow hydrodynamics and precipitation.

This report describes the application of two numerical codes to investigate the chemical reactivity of geothermal fluids during their exploitation. The codes (porousMedia4Foam and Drift-Flux) are coupling hydrodynamic and geochemistry and they are used to simulate the potential precipitation of different types of fluids. The main objective of this report is to present the capabilities of the code on different fluids with various properties: production of saline fluids at low temperature or hot fluids with low salinities. The chosen examples are inspired from real cases.

The results underline the ability of the codes to predict the nature of the deposits, but also their amount and the position into the facilities where the precipitation occurs. Analysis of the impact of geochemical uncertainties and flow properties on the scaling prediction of geothermal brine will enable operators to make a better decision about the operational settings and mitigation measures.

2 INTRODUCTION

Mineral scaling is one of the main challenges complicating the efficient operation of geothermal systems. The deposition of solid scales can lead to clogging of wells, reservoirs or surface facilities, reduction of flowrates within the wellbore and topside equipment, and impede the transfer of heat within heat exchanger systems, ultimately affecting the lifespan and economic viability of geothermal systems.

To avoid treating these deleterious physical and chemical reactions and their consequence on production operations, we need to use relevant numerical tools in order to predict these processes and to anticipate them before they occur.

This report summarizes the activities related to the application of predictive models to simulate the impact of fluid flow hydrodynamics and chemical composition uncertainties on the production behavior of geothermal assets. Codes developed in Tasks 4.1 and 4.2 of the H2020 REFLECT are used to simulate the hydraulic, thermal, and chemical behaviour of the fluid in the wells and surface facilities. Since precipitation typically occurs at pipe wall surfaces, efforts focused specifically on modelling deposits there. The understanding and the modelling of the growth of these deposits is crucial since it has an impact on the productivity performances of the wells.

In a first example, the porousMedia4Foam code is used on a high-salinity fluid with a moderate temperature. No phase change occurs during the pumping but because of the salinity of the fluids, deposits of barite are expected.

In a second example, the porousMedia4Foam is applied to a hot fluid with a lower salinity (with phase change). Based on the chemical composition of the geothermal brine, which depends on the geological formation and on the operational settings, different types and amounts of scales can form within the system, including calcite ($CaCO_3$), barite ($BaSO_4$), as well as silica scales (which are mainly observed in high-enthalpy systems). For these simulations, the thermo- and hydrodynamics of the system, i.e., the flowrates, pressures and temperatures, are used to determine the precise location and severity of scaling.

In a last example, the Drift-Flux code is used to simulate the mineral precipitation behavior of the geothermal fluid as both uncertainties in the fluid composition and the interaction between the fluid flow hydrodynamics and mineral precipitation can impact the deposition of the scaling.

3 APPLICATION OF POROUSMEDIA4FOAM

3.1 SIMULATOR DESCRIPTION

Simulations of scaling formation are run in this section with *porousMedia4Foam* – a multi-scale open-source hydro-geochemical simulation platform developed by the authors to model reactive transport phenomena at multiple scales i.e. at the pore-, hybrid- and Darcy-scales (Soulaine et al., 2021). *porousMedia4Foam* is built on the skeletal framework of OpenFOAM (*https://www.openfoam.org*) for solving for flow and transport and has been successfully coupled with PHREEQC to account for geochemistry (*https://www.usgs.gov/software/phreeqc-version-3*). The code is available at *https://github.com/csoulain/porousMedia4Foam*. A User's Guide to the software is available as REFLECT Deliverable 4.1 (see Pavuluri et al., 2021).

The package comprises of several flow solvers such as the 'constantVelocityFoam' – assigns a constant velocity field within the flow domain, 'dbsFoam' – solves the Darcy-Brinkman-Stokes equation and 'darcyFoam' – solves the Darcy's equations. *porousMedia4Foam* also includes an extensive set of models that describes the evolution of porous media and fluid properties.

In this study, we investigate flow and scaling formation, first at the scale of the well using a 1D approach, and then, using high-resolution 3D simulations to interrogate emerging processes at the junction between two segments of different diameters.

In the first case, governing equations are cross-section-averaged. The resulting equations form a Darcy-like system that is solved using *darcyFoam* solver. For an incompressible fluid, the mass balance equation in a well comprising of varying cross-sections (A_c) is given by,

$$\frac{\partial}{\partial z}\left(A_c v_f\right) = 0 \qquad [1]$$

where v_f refers to the fluid velocity defined by cross-section averaged momentum that looks like Darcy's law,

$$v_f = \frac{-k}{\mu}\left(\frac{\partial p}{\partial z} - \rho g_z\right) \qquad [2]$$

k is a friction factor that depends on the well diameter and flow rates, μ is the fluid viscosity and $\partial p/\partial z$ is the pressure gradient. The friction factor is computed by a Colebrook-White model. Though we are interested in 1D analysis, the cross-sectional area A_c is integrated into the mass balance equation (Eq. 1) to account for change in cross-sectional areas. Substituting Eq. 1 in Eq. 2 results in a Laplacian equation to be solved for the pressure. Once the pressure is computed, the velocity is calculated following Eq. 2, and transport equations for species are computed to update the concentration profile.

In the second case, we use Navier-Stokes-based simulations to investigate the saturation index at the vicinity of the corners of the expanding cross-section of the well. The simulation is performed in two consecutive steps. First, a steady-state Reynolds Average Navier-Stokes

(RANS) simulation based on k-Epsilon model is run with *simpleFoam*. Then, resulting velocity profile is used in *porousMedia4Foam* (using *constantVelocityFoam*) to transport chemical species and compute geochemistry.

For the geochemical calculations, we use the phreeqcRM geochemical package that acts as an interface between OpenFOAM and PHREEQC (Appelo and Parkhurst, 2013; Parkhurst and Wissmeir, 2015). The coupling between the packages relies on an operator splitting strategy. We use the Strangs algorithm in which advection-dispersion of chemical species is solved for half a time-step initially, the geochemistry for a full time-step, and the transport equation is computed for the remaining half time-step.

$$\frac{\partial C_i}{\partial t} + \nabla.\left(v_f C_i\right) - \nabla.\left(D_i.\nabla C_i\right) = 0 \qquad [3]$$

In the transport equation, C_i is the species concentration, D_i is the effective dispersion tensor that accounts for molecular diffusion and hydrodynamic dispersions. The geochemical time step is run by PHREEQC. The sequential order of steps followed in *porousMedia4Foam* is illustrated in the form of a flowchart shown in Figure 1.

The hydro-geochemical coupling strategy implemented in *porousMedia4Foam* has been extensively benchmarked against state-of-the-art reactive transport packages for well established cases (Soulaine et al., 2021; Pavuluri et al., 2022).

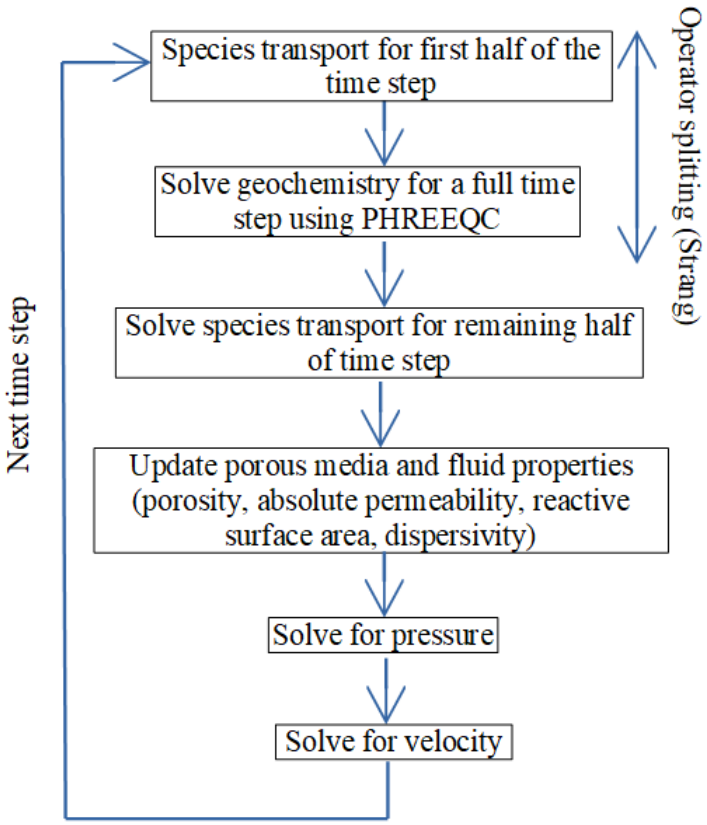

Figure 1: Sequential steps followed during solving a hydro-geochemical time step in *porousMedia4Foam*.

To model compressible multiphase flows, the mass conservation equations of the fluids in the system are described using the Darcys two-phase flow equations given by :

$$\epsilon \frac{\partial \rho_l S_l}{\partial t} - \nabla . \left(\rho_l \frac{k}{\mu_l} k_{r,l} (\nabla p_l - \rho_l g) \right) = q_l \quad [4]$$

$$\epsilon \frac{\partial \rho_g S_g}{\partial t} - \nabla . \left(\rho_g \frac{k}{\mu_g} k_{r,g} (\nabla p_g - \nabla p_c - \rho_g g) \right) = q_g \quad [5]$$

where ϵ is the porosity of the medium assumed to be equal to one in this report (ϵ = 1). ρ_i refers to the density of the fluid phase *i* where the subscript *i = g* refers to the gas phase and subscript *i = l* refers to the liquid phase, S_i refers to the fluid saturation, *t* is the time, v_i is the fluid velocity and q_i is the source/sink term of phase *i*. The gradient of the capillary pressure ∇p_c is used to link the pressure gradient between the two phases $\nabla p_c = \nabla p_a - \nabla p_b$. In the equations [4] and [5], the fluid phase velocity v_i is described using Darcy's two-phase flow equation given by Muskat and Meres (1936).

$$v_i = -\frac{k}{\mu_i} k_{r,i} (\nabla p_i - \rho_i g) \quad [6]$$

where *k* is the permeability of the medium, μ_i is the fluid viscosity, $k_{r,i}$ is the relative permeability of fluid *i*, ∇p_i is the pressure gradient and *g* is the acceleration due to gravity. Due to the presence of two fluids in a multiphase system, the displacement of one fluid is hindered due to the presence of another fluid in the medium which is indicated by the relative permeability $k_{r,i}$. The relative permeability of fluids appear in the Darcy flow (Eqs. 4 and 5) and are linked to the saturation of the medium.

The three unknowns in Equations 4 and 5 are the saturation of fluids S_g, S_l (with $S_g + S_l = 1$) and the pressure *p*. In Equations 4 and 5, we define mobility as $M_i = (k.k_{r,i})/\mu_i$ and the inertial term as $L_i = M_i$□$_i$. Summing Equations 4 and 5 results in the following:

$$\epsilon \left(\rho_l \frac{\partial S_l}{\partial t} + S_l \frac{\partial \rho_l}{\partial t} + \rho_g \frac{\partial S_g}{\partial t} + S_g \frac{\partial \rho_g}{\partial t} \right) - \nabla . (L \nabla p) = q \quad [7]$$

where $L = L_g + L_l$. In the above equation, the solutions density ρ_l is computed using equations of state implemented in PHREEQC.

Considering the gas phase compressibility □$_g = \partial \rho_g / \partial p$ substituting into Equation 7 and upon performing several mathematical manipulations,

$$\epsilon \left(\frac{\partial S_l}{\partial t} (\rho_l - \rho_g) + \alpha_g S_g \frac{\partial p}{\partial t} + S_g \frac{\partial \rho_g}{\partial t} \right) - \nabla . (L \nabla p) = q \quad [8]$$

Equations 5 and 8 are solved to obtain the liquid saturation S_g and the pressure *p*. To solve this set of equations fully implicit or semi-implicit approaches can be used. The fully implicit approach is unconditionally stable therefore larger time steps can be used. However, the matrix to be solved is large and hence requires longer computation times. On the other hand, semi-implicit approach reduces the size of the matrix being solved however, requires use of

smaller time steps due to the partially explicit nature of the problem. In *porousMedia4Foam* we use the semi-implicit approach attributed to the sequential nature of workflow used in OpenFOAM.

We use the IMPES - IMplicit Pressure Explicit Saturation- method to solve the set of equation. Eq. (5) is solved explicitly based on the pressure values calculated at the previous time step. Based on the computed liquid saturation, the relative permeability of the fluids $k_{r,i}$ are computed according to Equations 4 and 5. Later, Equation 8 is solved implicitly to compute the pressure and Equation 6 is used to determine the velocity of fluids v_i. The computed fluid velocities are then used for solving the transport of species. The above discussed solution for compressible multiphase flow is implemented in the compressibleDarcyFoam flow solver of *porousMedia4Foam* package.

3.2 APPLICATION TO GEOTHERMAL WELL: A SIMPLE CASE

The first example presented in this report is inspired from the fluid produced at the Heemskerk site (NL). The Dutch company Floricultura BV intends to use the geothermal capacity from the deep wells to heat their Heemskerk greenhouse facilities, covering about 10 hectares. For that, two wells (HEK-GT-01 and HEK-GT-02) of the geothermal doublet are drilled from the same location. The wells were drilled in the Slochteren sandstone formation reaching depths over 2,600 m vertical from the surface. The Slochteren sandstone formation is the reservoir that is deployed for providing the geothermal heat (Figure 2).

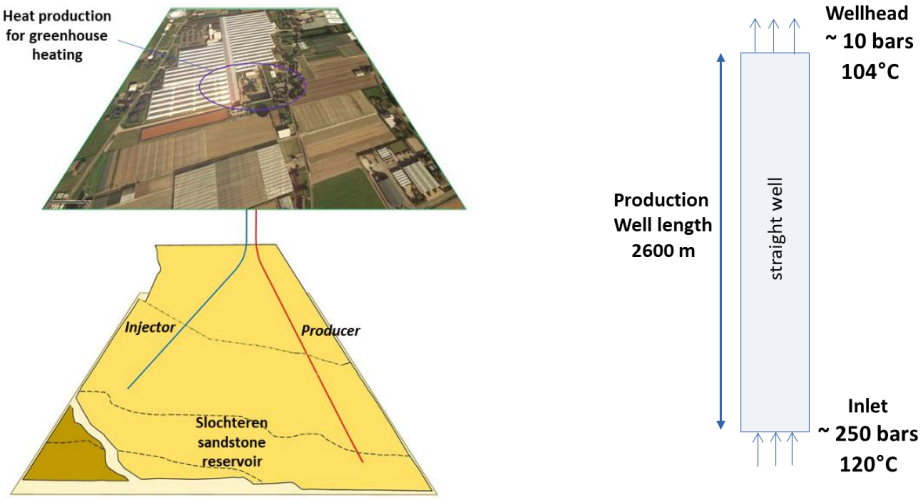

Figure 2: Geothermal system from Heemskerk (from https://wellengineeringpartners.com).

The production well is considered as straight with a constant diameter of 0.244 m and a length of 2,600 m (Figure 2). The geometry of the well allows testing the code on a simple application case. The well is discretized according to a 1D approach, with cells of same volume. The reservoir temperature is 116.5°C, whereas bottom pressure is 295 bar. Wellhead pressure is 12 bar and surface temperature is 104.5°C. According to temperature and pressure conditions at the boundaries of the well, the fluid is supposed to remain under liquid phase (no degassing). We consider a linear temperature gradient in the well between the feedzone and

the wellhead. The inlet and outlet pressure and temperature are constant all along the simulation. The discharge flow is 80 kg.s^{-1}. The fluid velocity is estimated from the pressure gradient to about 0.39 m.s^{-1}. It is constant all along the well and the impact of fluid density variations is negligible.

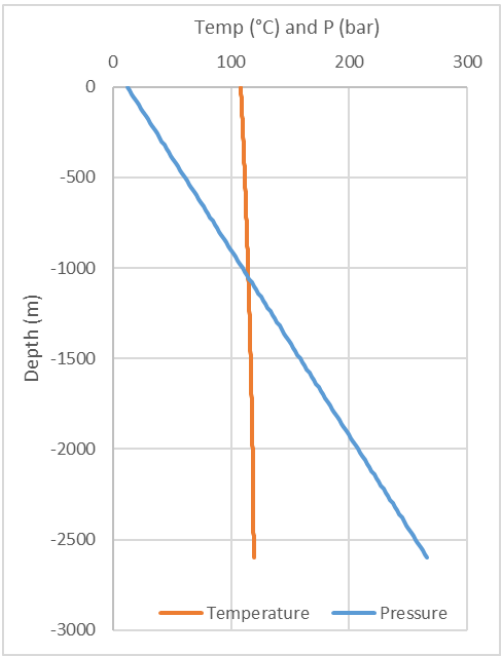

Figure 3: Temperature (in red) and pressure (in blue) profiles in the production geothermal well.

The geothermal fluid is a brine with a salinity close to 260 g.L^{-1}. The high salinity involves a fluid density close to 1.109 in the reservoir conditions. The pH is acid with a value close to 4.58 and a redox potential of -130 mV. It is here supposed that the fluid at equilibrium with respect to barite and undersaturated with respect to main minerals such as calcite and quartz (Figure 4). Barite is the main mineral investigated in these fluids since it is identified as a potential scaling problem (Hartog, 2015).

Table 1: Chemical composition of the fluid produced at Heemskerk site (Pers. Comm. L. Walsh)

Elements	Concentration (mol/kgw)
pH	4.576 (unitless)
Ba	1.07E-04
C	1.09E-02
Ca	2.37E-01
Cl	4.51E+00
Fe	2.22E-03
K	2.07E-02
Li	4.48E-03
Mg	4.94E-02
Mn	1.88E-04
Na	3.91E+00
S	4.04E-03
Si	1.56E-04
Sr	5.02E-03

Then, we perform reactive transport calculations. It is supposed that the production well only contains pure water initially. The formation fluid is produced only at the bottom of the well at a constant flow rate.

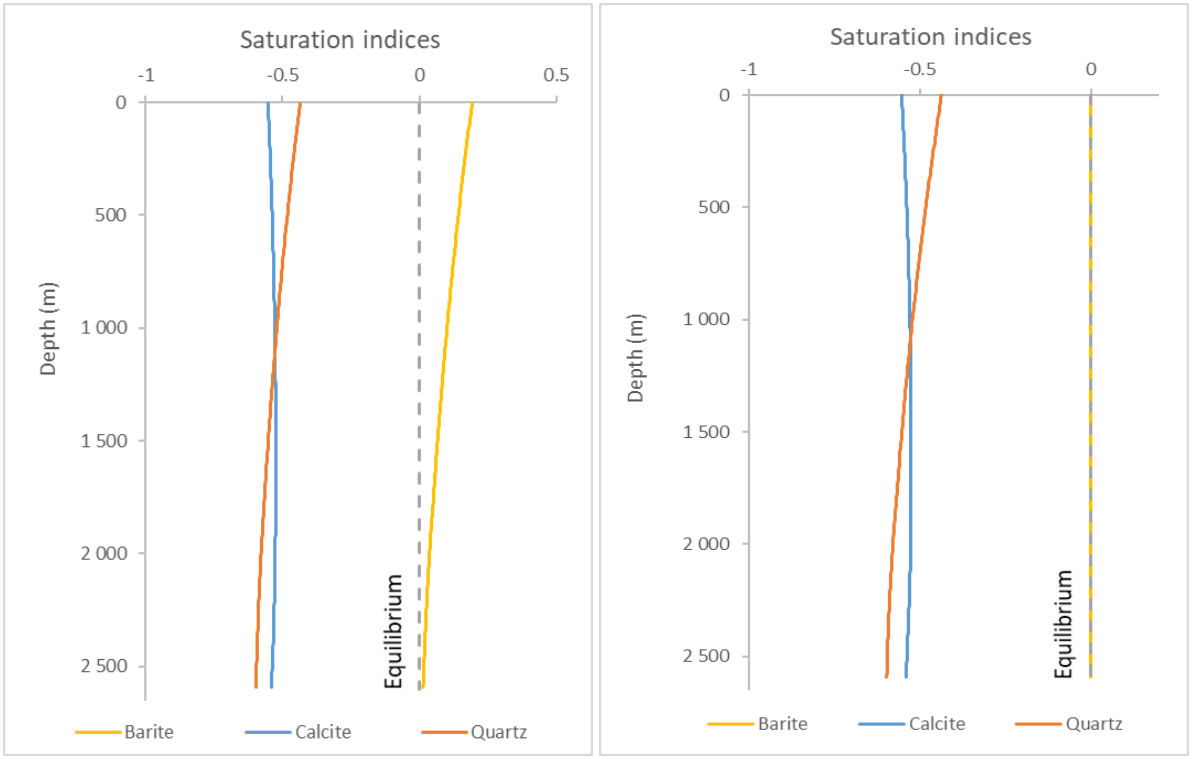

Figure 4: Saturation indices of quartz, calcite and barite in the well. Left, no reactivity assumed. Right, equilibrium with mineral phases assumed

A first simulation allows studying the evolution of the saturation indices along the well. By decreasing temperature, saturation indices of quartz and barite increases (Figure 4 - left). If quartz remains undersaturated in the solution, barite is oversaturated (Figure 4 - left). A second simulation is then proceeded by activating precipitation of minerals (Figure 4 - right). Since barite is oversaturated, this mineral precipitates along the well and the deposited amounts of mineral can be estimated (Figure 5). By using equilibrium constraints on the oversaturated minerals, a peak is observed in the first cell (Figure 5 - left). It is because barite is not exactly in equilibrium in the reservoir (SI = 0.013). And since equilibrium constraint is assumed in the well, barite massively precipitate in the first cell.

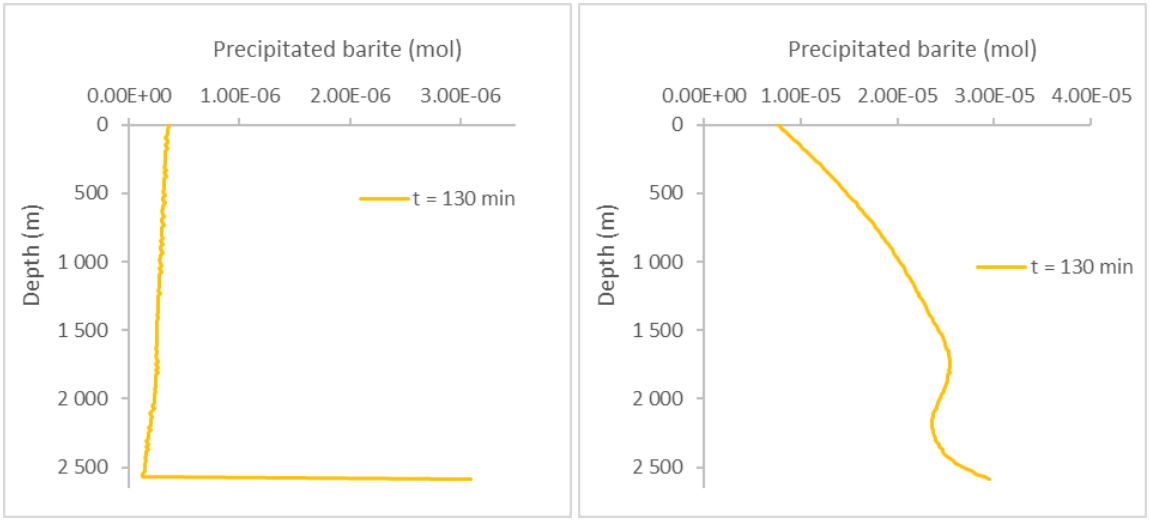

Figure 5: Amount of barite precipitated in the well after one renewing of the well volume: equilibrium (left) and kinetic approach (right)

This artefact can be solved by using kinetic constraint. A last run is made considering a precipitation kinetic for barite. The parameters for the kinetic law are issued from Palandri and Kharaka (2014). With this constraint, the barite precipitation spreads on many cells avoiding the peak in the first cell (Figure 5 - right).

3.3 APPLICATION TO GEOTHERMAL WELL WITH A MORE COMPLEX GEOMETRY

The objective of the second example is to apply the model to a saline and hot fluid (Temperature higher than 150°C). For that, we inspired from geothermal wells exploiting the Tuzla Geothermal Field. Indeed, this field, located in an active tectonic zone on the Biga Peninsula in Northwestern Turkey, produces saline geothermal fluids with temperature close to 173°C (Baba and Tonkul, 2022; Tonkul et al., 2022). For this specific application case, we used the characteristic dimensions of the well T9, 540 meters deep and made of three segments of different cross-sections whose dimensions are shown in Table 2 (Baba et al., 2009).

Table 2: Geometric dimensions of the geothermal well. The feedzone of the well is located at 540 m and wellhead is at 0 m

Well Interval	Length [m]	Cross-section diameter [m]
0 m – 49 m	49	0.50
49 m – 220 m	171	0.35
220 m – 540 m	320	0.25

The fluid exploited is a geothermal brine analysed at the surface. The chemical composition is given in Table 3. These fluids are produced from the deep geothermal reservoir and they are highly chemically modified when they are reaching the surface. The waters are degassing and they are cooled. In the reservoir, the temperature and pressure are about 160°C and 50 bar, respectively.

Table 3: Chemical composition of the geothermal brine produced from Well T9 (Baba et al., 2009). Concentrations of elements are given in mg/L

Temperature (°C)	25
pH	6.21
pe	-3.5
Ca	2560
Mg	122
Na	17950
K	2210
Cl	34840
Alkalinity (as HCO_3)	135
SO_4	227.4
S^{-2}	79.4
SiO_2	176
F	4.22
Ba	6.23
Sr	130
Sb	0.06
Pb	0.005

The first step consists in estimating the chemical composition of the brine in the reservoir, i.e. before any chemical modification due to brine exploitation. To do that, the temperature and the pressure of the fluids are increased up to the reservoir's conditions (in this case 160 °C and 50 bar). Then a last constraint is imposed to the fluid: it is assumed that the fluid is in equilibrium with carbonates (and more specifically with calcite). To impose this constraint, the CO_2 partial pressure is adjusted: in this case, a value of 2.5 bar is used. This constraint is realistic since it is supposed that the fluids are generally in a thermodynamic equilibrium with carbonates present in formation rocks.

Two sets of simulations are considered. First, the saturation index is computed in a one-dimensional (1D) well using a cross-section-averaged formulation (Darcy-like). Second, we use high-resolution modelling using Navier-Stokes-based Direct Numerical Simulations (DNS) to investigate the impact of turbulent flow mechanisms on the scaling formation at the junction of two well segments of different diameters.

3.3.1 One-dimensional calculations

Calculation is done with *porousMedia4Foam*. The well is discretised by 540 cells along the length of the channel ($\Delta y = 1\ m$). The three different cross-sectional areas of the well have been assigned to the setup according to the data provided in Table 3. The friction coefficient is computed through the cross-section diameter and the flow rate using the Colebrook-White formula.

According to the available field data, the feedzone is set a Dirichlet boundary condition for pressure $p_{feedzone} = 50\ atm$ and $p_{wellhead} = 3\ atm$. The velocity at the boundaries is a zero gradient Neumann boundary. The temperature at the feedzone is $T_{feedzone} = 160°C$ and $T_{wellhead} = 139°C$.

The fluid viscosity and density are μ = 0.001 kg/m.s and ρ=1000 kg/m^3, respectively.

First calculations are done with *porousMedia4Foam*. However, despite all the efforts done to implement the multiphase flows, the code is not able to predict the degassing inside the well. For the time being, we used the code to solve a single phase problem, without considering any degassing. Only the pressure and temperature are changing according to depth and the saturation indices of three minerals (barite, calcite and quartz) are followed inside the well.

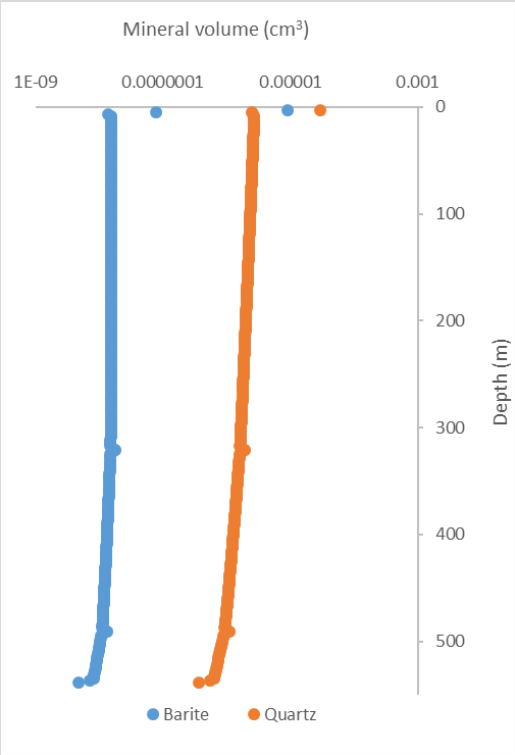

Figure 6: The volume of barite (blue) and quartz (orange) according to the depth on the geothermal production well

Figure 6 shows that barite and quartz precipitate in small amounts all along the production well, mainly in relation with the temperature decrease. But, since the degassing is not modelled, the saturation index of calcite decreases and this mineral does not precipitate.

To model the behaviour of calcite, we performed another simulation. Figure 7 shows the pressure and temperature profiles in the geothermal well calculated with GWELL code (Aunzo et al., 1991). The pressure drop is more pronounced in the thinner cross-section of the well due to larger viscous dissipation. On the other hand, the thicker cross-section of the well shows a lower pressure drop due to lesser viscous dissipations. The impact of degassing in the well can be observed on the temperature profile: temperature suddenly decreases at 100 m depth because of phase change.

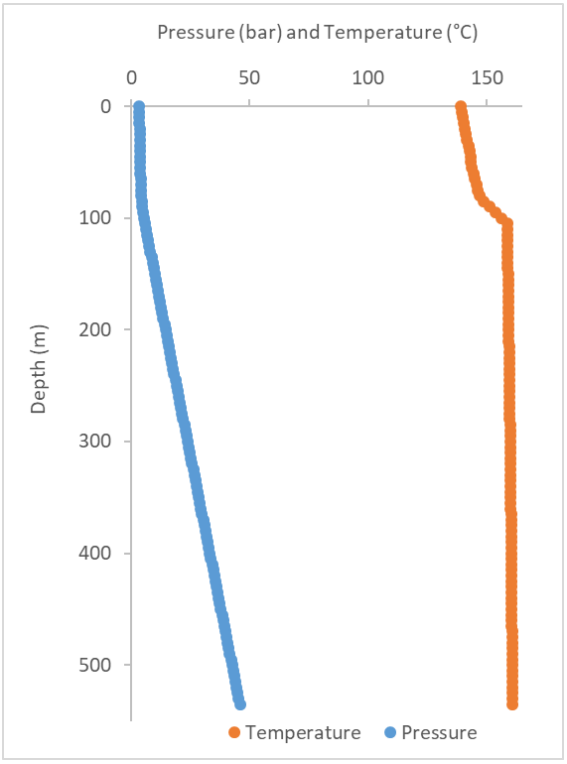

Figure 7: The pressure (blue) and temperature (orange) profiles in the geothermal production well

Then the temperature and pressure profiles calculated with GWELL code are implemented in PHREEQC code in order to simulate the chemical reactivity in the well. For the specified solution composition given in Table 3, there exists potential to precipitate calcite ($CaCO_3$), quartz (SiO_2), galena (PbS)and barite ($BaSO_4$) within the well. Indeed, the saturation indices of these minerals increase along the production well when the fluid raise the surface.

The degassing involves a sharp pH increase, which is due to the exsolution of CO_2 (Figure 8).

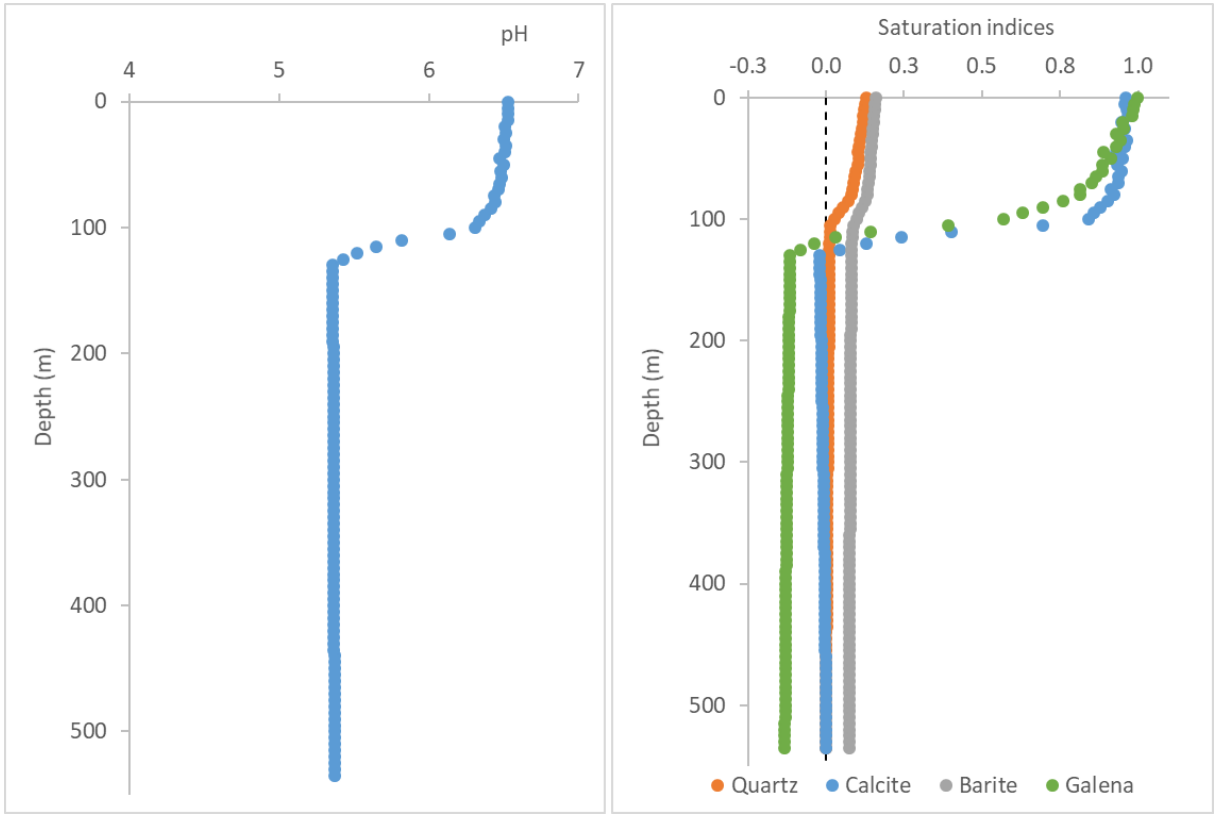

Figure 8: left: pH profile according to depth. Right: saturation index profile for minerals – calcite (blue), quartz (orange), galena (green) and barite (grey) in the geothermal production well. The dashed black line indicates equilibrium (saturation index of 0) for reference.

The saturation index of calcite (shown in continuous blue line-Figure 8) increases towards the wellhead. First close to the equilibrium in the lower part of the well, it becomes positive at 100 m depth indicating that calcite is oversaturated and ready to precipitate within the well. This sudden increase is mainly due to the degassing. CO_2 is exsolved and pH increases involving the oversaturation of calcite and the risk of calcite precipitation. On the other hand, quartz is more soluble at high temperatures. Hence, the saturation index of quartz (shown in orange-Figure 8) rises towards the wellhead. Close to the feedzone, the saturation index of quartz is close to zero. Moving towards the wellhead, the saturation index of quartz increases indicating oversaturation of this mineral in the well and a potential precipitation, mainly in the upper part of the well. Barite shows the same behaviour as quartz. About sulphide mineral, galena is initially undersaturated in the reservoir with respect to the solution. It remains undersaturated in the lower part of the well. However, when degassing occurs, its saturation index becomes positive with risks of precipitating such mineral. This is probably due to pH change and also the release of H_2S in the gaseous phase (see Figure 9).

Then, the thermodynamic equilibrium of the solution is assumed with respect to these four minerals. The code can calculate the amount of precipitated minerals. The gas composition can also be calculated, supposing it contents $CO_{2(g)}$, $H_2O_{(g)}$ and $H_2S_{(g)}$. Figure 9 shows that calcite precipitates after the degassing. The raising of the temperature involves also the precipitation of quartz. Barite precipitates in very small amounts as well as galena. Concerning the gaseous phase, it is mainly composed of vapour but, CO_2 and H_2S are also composing it in small amounts.

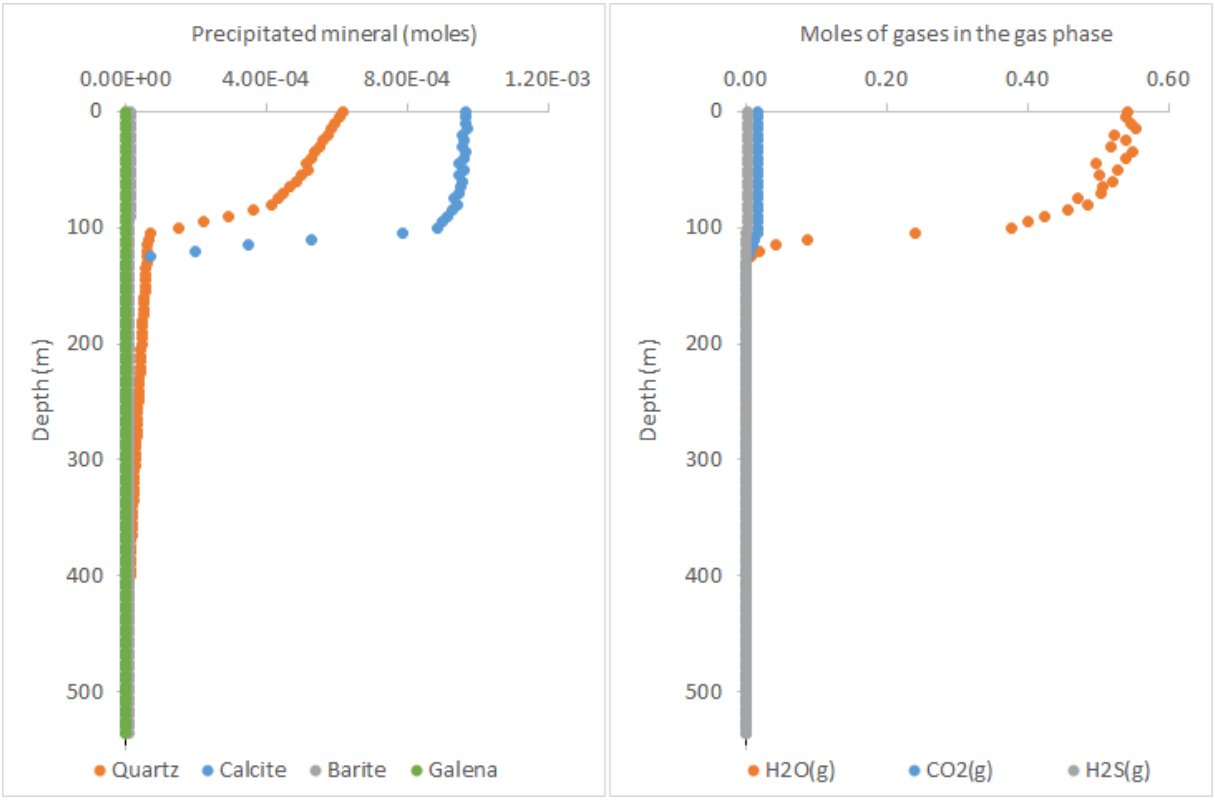

Figure 9: Left: amount of precipitated minerals according to depth. Right: number of moles of gases in the gaseous phase in the geothermal production well.

In conclusion, this simulation shows that all the saturation indices remain close to 0 and low amounts of precipitated minerals are expected before the degassing point estimated to about -105 m. The degassing drastically influences the chemistry of the fluids and the model predicts the deposition of mainly calcite and traces of galena, barite and quartz. The model cannot predict the evolution of the thickness of the deposits (even if we can estimate the volume of minerals – results not shown here) but it gives information on the composition of the scaling. These results are compared with the observations done on the site by Demir et al. (2014). These authors characterized the composition of scaling in some wells of the Tuzla Geothermal Field. Their investigations focused on deposits recovered from the surface to a depth of 75 m in the well. According to their elemental analysis, they are mainly composed Pb, Fe, Mg, Ca and Si (Figure 10). The author confirmed that Ca is mainly present in calcite and aragonite according to the depth, whereas Pb is present in galena. About silica, they observe an increase of the proportion close to the surface, which could be due to lower temperatures. All these field observations are fully consistent with the numerical results.

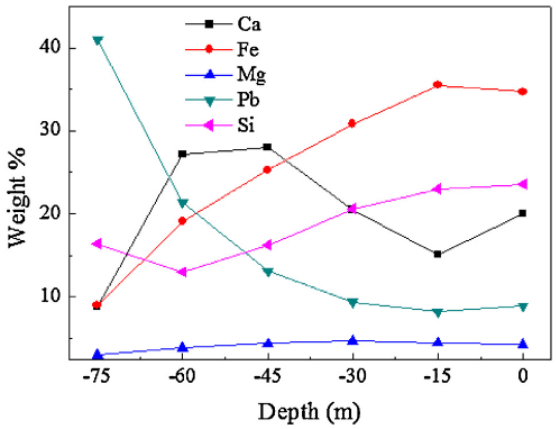

Figure 10: Elemental composition of scales in the well obtained by XRF as a function of height the scale collected. The samples are collected from the surface of inhibitor hose (From Demir et al., 2014)

3.3.2 High-resolution simulations observations

The impact of hydrodynamics on the scaling formation at the change of cross-section has received little attention so far. We use Navier-Stokes-based simulations to interrogate emerging processes in this area of the well.

The geometry consists in a 2m long subset of the geothermal well #2 centered on the change of diameter from 0.5 to 0.35 m. It is described by a 2D axisymmetric domain meshed with 9800 hexahedral cells with refinement near the walls. A constant velocity of 0.44 $m.s^{-1}$ is applied at the bottom boundary. The top boundary has a fixed pressure value (0 Pa). No-slip conditions is used on the walls. We use the k-Epsilon model to compute turbulent flow in the well. The resulting steady-state velocity profile is then used in our coupled hydrogeochemical package to compute the geochemistry.

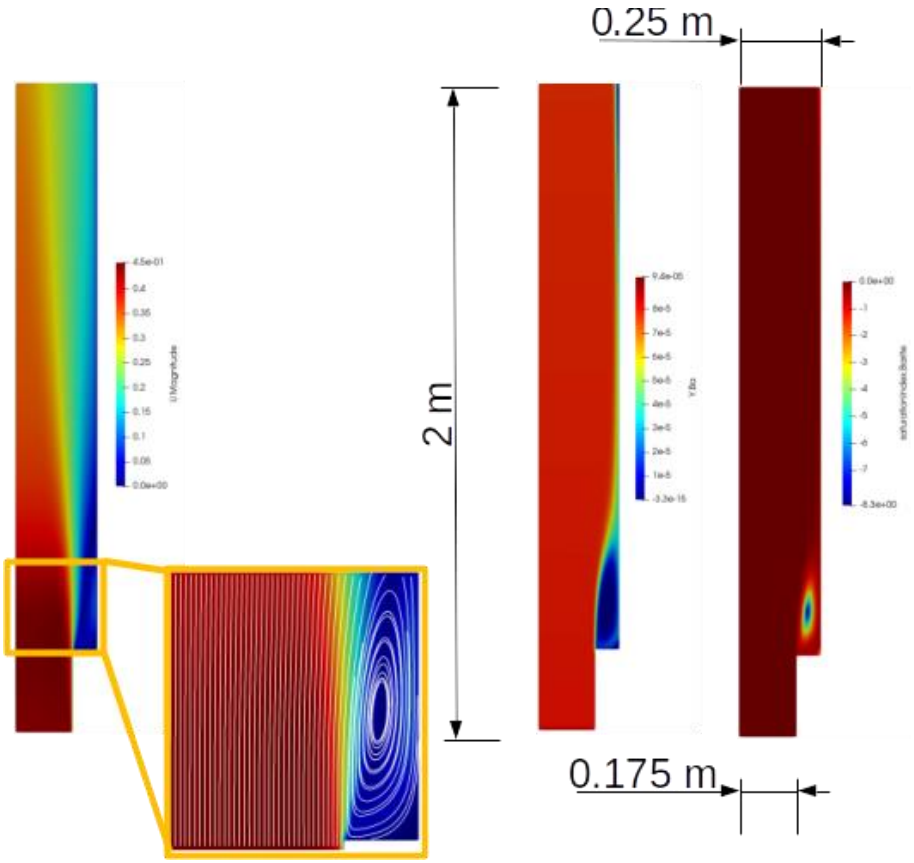

Figure 11: Left: flow profile in the well where the cross-section expands with vortices developed at the corners of the expanding cross-section of the well. Right: Barium concentration profile and barite saturation index

Typical results are shown in Figure 11. As expected, we observe a fluid recirculation at the corners of the expanding cross section of the well. These corner zones act as mixing zones for the chemical species. Re-circulation could modify chemical concentrations in the fluid and impact the saturation indices of precipitable minerals (we only show barite saturation index in Figure 11). The corner zones are therefore a favourable location for the creation of seeds that move inside the well, eventually. These disseminated seeds can then become ideal precursors for larger precipitations.

4 APPLICATION OF DRIFT-FLUX MODEL

4.1 SHORT SIMULATOR DESCRIPTION

A modelling workflow was developed to simulate the fluid flow behaviour in the geothermal assets by coupling the fluid flow and chemistry related processes. The schematic of the models and their integration is shown in Figure 12. A detailed description of the model and workflow is provided in Poort et al. (2022). An example code to perform uncertainty quantification with geo-chemistry modelling using PHREEQC was also provided as a supplementary document for D4.3 which can be found here: https://github.com/poortjp/REFLECT_D4-3_example. The model requires the geometry description, process boundary conditions (such as reservoir pressure and temperature and top-side constraints) and brine composition. The flow properties such as superficial velocities and volume fractions of phases and process conditions are being calculated by Drift-Flux model. After the flow is calculated, the local information will be used to calculate the scaling and saturation index at various locations of the geothermal asset to estimate the risk of scaling locally. Other flow-chemistry issues such as corrosion could also be estimated using this model, e.g. by tracking the pH value of the brine at different locations.

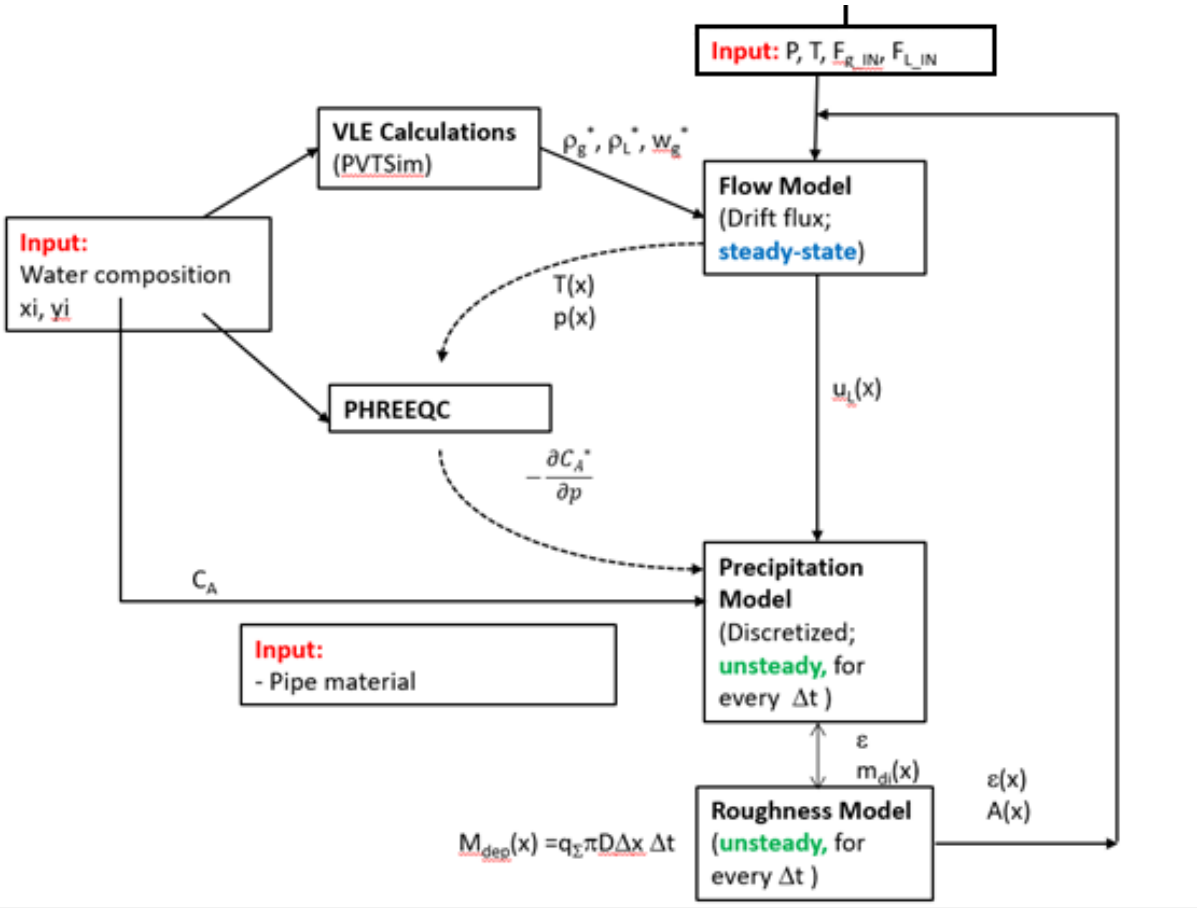

Figure 12. Workflow of the coupled flow-chemistry modelling framework. Image adapted from Twerda 2014

Due to a relatively low computational cost of the model, it can be used to simulate the full geothermal plant and provide insights on the production behaviour and potential risks including the uncertainties in the fluid composition and process conditions. For this purpose, an uncertainty quantification workflow (schematic shown in Figure 13) was integrated with the solver to quantify the impact of uncertainties in the brine composition and process conditions on the simulated variables. The model will be treated as a deterministic model to only focus on the impact of aleatory uncertainties on the prediction. For the sampling, there are several techniques such as Monte-Carlo, Latin Hyper Cube and collocation methods, the latter of which is suited for computationally expensive simulators.

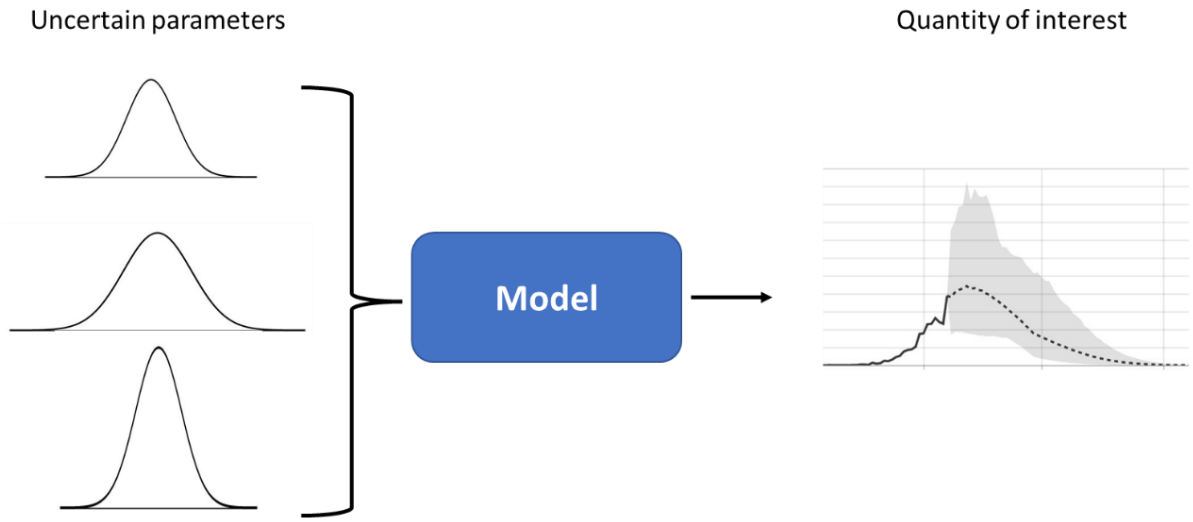

Figure 13. Uncertainty propagation over a deterministic model to estimate the impact of aleatory uncertainties

4.2 APPLICATION

In order to demonstrate the application of the developed models, a low-enthalpy geothermal doublet system was simulated. The geothermal system was assumed to produce with the production temperature of around 100°C. The water is produced from a reservoir with the pressure of 300 bars at the depth of 3 km. The full plant was modelled from the producer well to filter, heat exchangers, injector pump and injection well. In this case, the doublet can be operated at different surface pressure to allow for different level of gas dissolution in the brine. The simulated case was inspired by the Heemskerk geothermal field in the Netherlands due to its high production temperature (relative to Dutch geothermal doublets) and not having any gas-liquid separator on the surface facilities.

The list of elements in the brine composition and uncertain parameters and their assumed uncertainty range in their composition is shown in Table 4. Latin hypercube sampling was used to sample from the uncertain parameters.

Table 4. List of brine ions which were varied in the uncertainty analysis framework

Elements	Concentration [mg/l]	Min/max percentage uncertainty
Na	85000	
K	2200	
Ca	7450	±3%
Mg	1150	
Ba	5.5	±3%
Sr	290	±3%
Fe	175	
Cl	145000	±3%
S(6)	585	±4%
Mn	9.25	

A series of calculations for different conditions were performed with the simulator which two of the cases for allowing 0% and 1% gas in the system are shown in Figure 14 and Figure 15 for pressure and gas volume fraction, respectively. The results showed that the pressure was not impacted much in the production and injection well. A decline in the pressure in the surface piping is observed due to the presence of heat exchanger and filter and at the normalized length of 0.7 the pressure is increased by a booster pump. Higher head was estimated for the case with higher gas fraction. Regarding the volume fraction of the gas, not much gas was observed in the production well, except for the area very close to the wellhead and on the surface the gas fraction variation which is dependent on the pressure and temperature is captured.

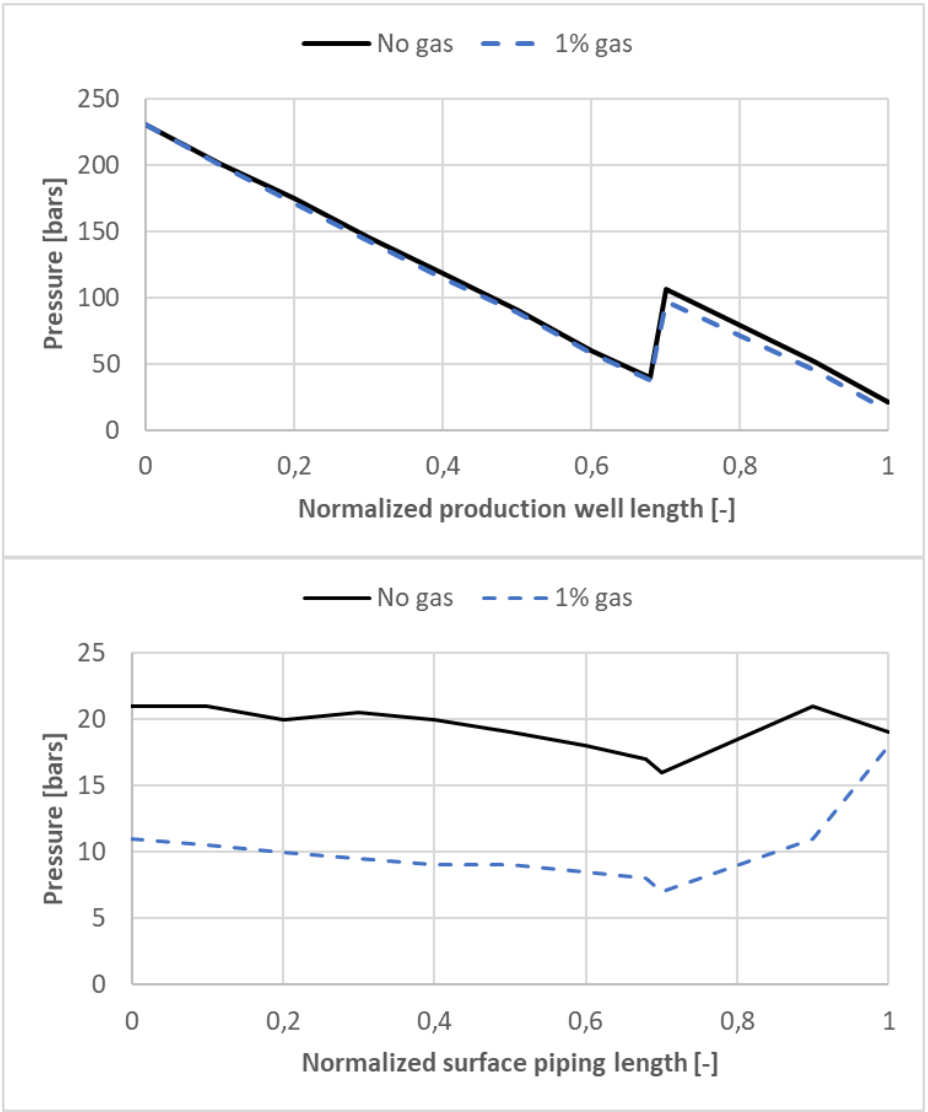

Figure 14. The pressure profile for two cases of 0% and 1% gas in the system along the geothermal production well and surface piping. All the results are shown by normalizing the length of the wells and pipes.

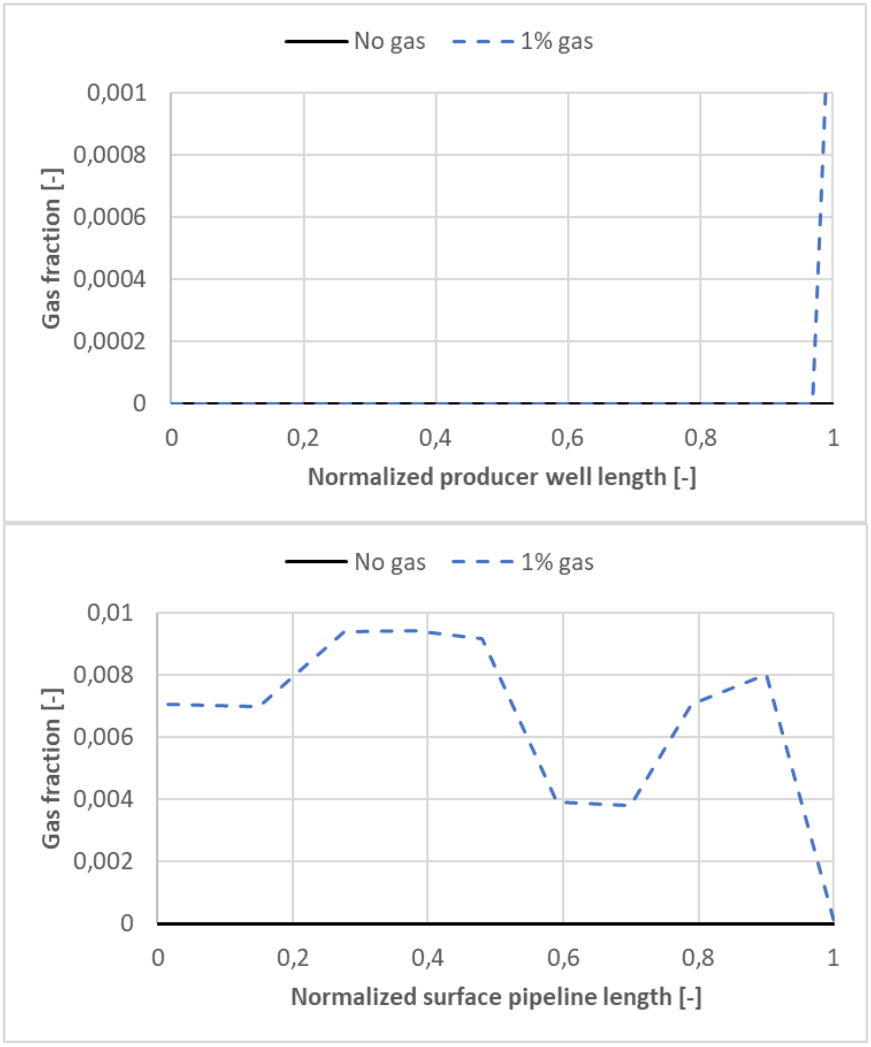

Figure 15. The gas fraction (volumetric) for two cases of 0% and 1% gas in the system along the geothermal production well and surface piping. All the results are shown by normalizing the length of the wells and pipes.

Following by the calculation of the flow field, the uncertainty quantification workflow coupled to the simulator to estimate the scaling potential at various location of the geothermal plant. The scaling potential for Calcite, Barite and Celestite along the production well and surface piping is shown in Figure 16 and Figure 17, respectively. The simulations managed to estimate the evolution of saturation indices for three example minerals, including calcite, barite and celestite. In the production well, the probability of barite formation is increasing more towards the surface but uncertainties in the brine composition will not lead to a barite precipitation downhole of the production well. The probability of the calcite formation was not impacted by the brine composition uncertainties. In the surface piping barite, celestite and calcite are oversaturated which by further reduction in the pressure and temperature over the filter and heat exchanger, the calcite and celestite saturation is decreased. Barite scaling index is still 0 even after the heat exchanger due to the temperature dependency of the barite precipitation. Most importantly, the scaling indices on the surface piping and facilities were not significantly impacted by the brine composition uncertainties. This workflow, in addition to the previously available workflow proposed by Wasch et al. (2019) will provide the probability of the scaling at different location of the plant considering brine composition and process conditions uncertainties.

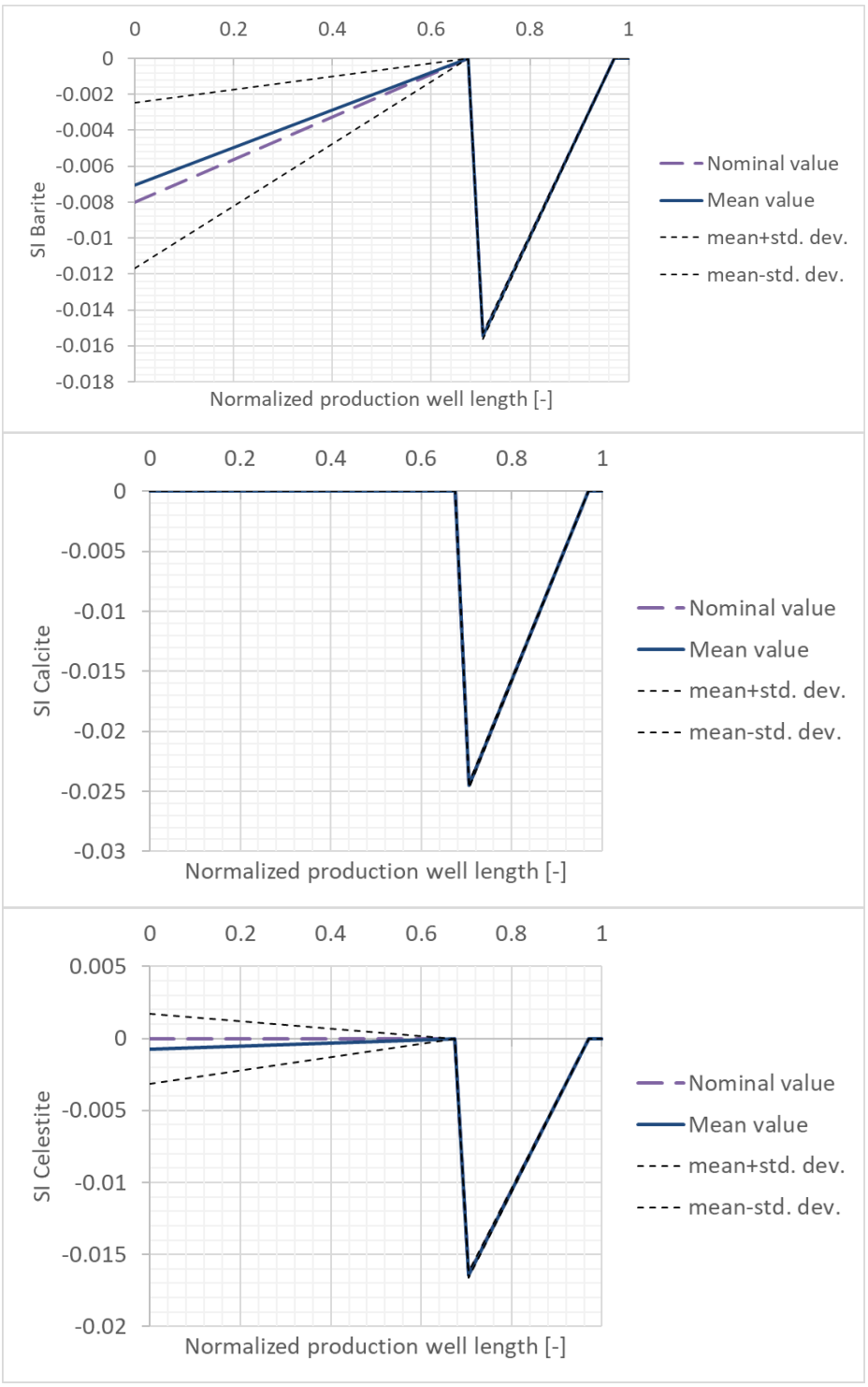

Figure 16. Scaling index of Barite, Calcite and Celestite along the production well considering the uncertainties in the brine composition

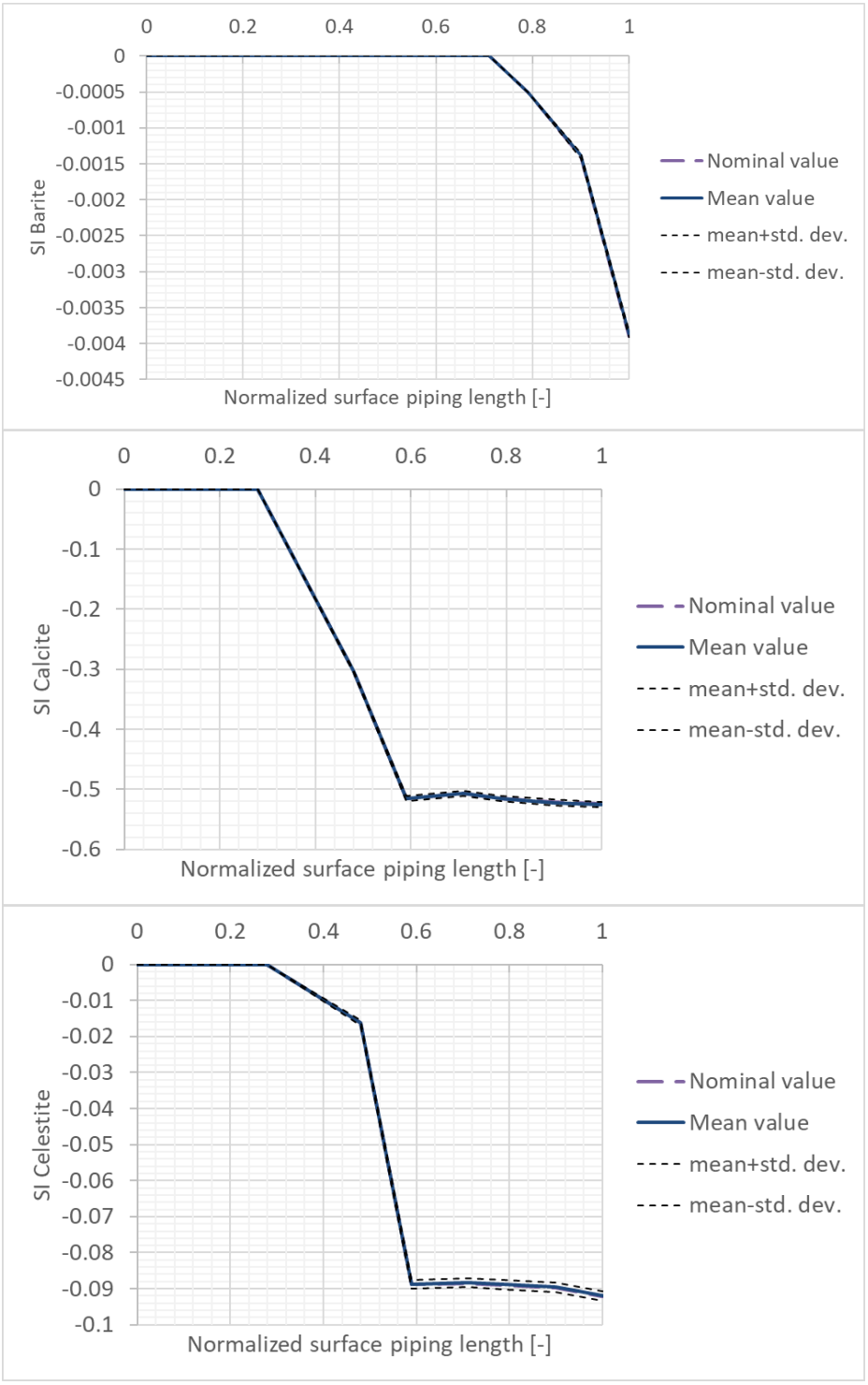

Figure 17. Scaling index of Barite, Calcite and Celestite along the surface piping considering the uncertainties in the brine composition

5 CONCLUSIONS

This report presents the capabilities of two coupled hydrodynamic and geochemical codes: porousMedia4Foam and Drift-Flux.

PorousMedia4Foam code is enable to simulate the transfer of fluids in pipes according to Darcy or Navier-Stockes approaches. It allows simulating the precipitation of minerals in geothermal tubings according to temperature and pressure gradients. It can predict the nature and the amount of the scaling in straight wells or wells with different diameter sections. The use of Navier-Stokes-based simulations allows estimating the impact of hydrodynamics on the scaling formation at the change of cross-section. However, even if this code has been tested on many application cases, additional developments are still needed. The main one is about the implementation of the modelling of multiphase system. Indeed, the prediction of the phase change in the well during the production must still be improved to accurately simulate the reactivity ion the hot geothermal systems.

Drift-Flux code was developed to simulate the fluid flow behaviour in the geothermal assets by coupling the fluid flow and chemistry related processes. From the geometry description, process boundary conditions (such as reservoir pressure and temperature and top-side constraints) and brine composition, the code calculates the flow properties such as superficial velocities and volume fractions of phases and process conditions and finally the scaling and saturation index of minerals at various locations of the geothermal asset. In this report, the code is applying uncertainties on the concentrations of dissolved elements in order to estimate the impact on the nature and the amount of scaling. This tool is of main interest for operators to anticipate the chemical processes responsible of scaling in facilities.

6 REFERENCES

Aunzo, Z.P., Bjornsson, G., Bodvarsson, G.S. (1991). Wellbore Models GWELL, GWNACL, and HOLA. User's Guide. LBL-31428 – UC 251. October 1991.

Baba, A., Yuce, G., Deniz, O., Ugurluoglu, D.Y. (2009). Hydrochemical and isotopic composition of Tuzla geothermal field (Canakkale-Turkey) and its environmental impacts. *Environmental Forensics* 10(2): 144-161. http://dx.doi.org/10.1080/15275920902873418

Baba, A., Tonkul, S. (2022). The H2020 REFLECT project: Deliverable 1.2 - Conceptual model for the Tuzla geothermal site, GFZ German Research Centre from Geoscience. https://doi.org/10.48440/gfz.4.8.2022.006

Demir, M.M., Baba, A., Atilla, V., Inanlı, M. (2014). Types of the scaling in hyper saline geothermal system in northwest Turkey. Geothermics 50, 1–9. https://dx.doi.org/10.1016/j.geothermics.2013.08.003

Hartog, N. (2015). Geochemical Assessment of Injectivity Problems in Geothermal Wells - A Case Study for several Greenhouse Geothermal Systems in The Netherlands. KWR 2015.012 | January 2015

Muskat, M., Meres, M.W. (1936). The flow of heterogeneous fluids through porous media. *Physics*, 7(9):346–363. https://doi.org/10.1063/1.1745403

Parkhurst, D.L., and Appelo, C.A.J. (2013). Description of input and examples for PHREEQC version 3—A computer program for speciation, batch-reaction, one-dimensional Transport, and inverse geochemical calculations: U.S. Geological Survey Techniques and Methods, book 6, chap. A43, 497 p., available only at http://pubs.usgs.gov/tm/06/a43/

Parkhurst, D.L., Wissmier, L. (2015). PhreeqcRM: A reaction module for transport simulators based on the geochemical model PHREEQC. *Advances in Water Resources* 83: 176-189. https://doi.org/10.1016/j.advwatres.2015.06.001

Pavuluri, S., Claret, F., Tournassat, C. and Soulaine, C. (2022). Reactive transport modelling with a coupled OpenFOAM®-PHREEQC platform. *Transport in Porous Media* 145: 475–504. https://doi.org/10.1007/s11242-022-01860-x

Pavuluri, S., André, L., Tournassat, C., Claret, F., Soulaine, C. (2021). The H2020 REFLECT project: Deliverable 4.1 - User's Guide of a Coupled Hydro-Thermal-Chemical Code for Fluids, Potsdam : GFZ German Research Centre for Geosciences, 55 p. https://doi.org/10.48440/gfz.4.8.2021.002

Poort, J., de Zwart, H., Wasch, L., Shoeibi Omrani, P. (2022). The H2020 REFLECT project: Deliverable 4.3 Impact of geochemical uncertainties on fluid production and scaling prediction. GFZ, German Research Centre for Geosciences, DOI:10.48440/gfz.4.8.2022.001

Soulaine, C., Pavuluri, S., Claret, F., and Tournassat, C. (2021). *porousMedia4Foam*: Multi-scale open-source platform for hydro-geochemical simulations with OpenFOAM®. *Environmental Modelling & Software* 145: 105199. https://doi.org/10.1016/j.envsoft.2021.105199

Tonkul, S., Baba, A., Demir, M.M., Regenspurg, S., Kieling, K. (2022). 3D Modelling and Characterization of Scale Types in Hyper Saline Geothermal System in Tuzla Geothermal Power. European Geothermal Congress 2022, Berlin (Germany), 17-20 Oct 2022.

Twerda, A., Veltin, J. (2014). Building blocks of asphaltene modelling: A combination of sub-models to quickly assess mitigation strategies. *s.l., s.n*.

Wasch, L., Shoeibi-Omrani, P., Twerda, A. (2019). Integrated Scale Management for Geothermal. In Proceedings of the European Geothermal Congress (Vol. 6).